RSC Advances

PAPER

View Article Online
View Journal | View Issue

Cite this: *RSC Adv.*, 2019, **9**, 41447

Step-by-step monitoring of CVD-graphene during wet transfer by Raman spectroscopy†

Zehao Wu,[a] Xuewei Zhang,[a] Atanu Das,[a] Jinglan Liu,[a] Zhenxing Zou,[a] Zilong Zhang,[a] Yang Xia,[b] Pei Zhao *[a] and Hongtao Wang*[a]

Received 5th November 2019
Accepted 8th December 2019

DOI: 10.1039/c9ra09268d

rsc.li/rsc-advances

Transfer acts as a crucial bridge between the chemical vapor deposition (CVD) synthesis of large-scale graphene and its applications, but the quality evolution of a graphene film during transfer remains unclear. Here we use scanning Raman spectroscopy to monitor as-grown graphene during each step of wet transfer including floating on etchant solution, loaded onto a target substrate, and with additional annealing. Results show that the etchant solution results in strong compressive strain and p-type doping to floating graphene, but both are significantly reduced after the sample is loaded and rinsed especially for the doping. An annealing treatment increases the compressive strain in graphene but hardly its doping level. Moreover, when a poly(methyl methacrylate) (PMMA) layer is used to assist the transfer, it does not only increase the p-type doping of floating graphene but also lowers the crystalline quality of annealed graphene. Therefore, to obtain graphene with better quality, besides the attempts of improving CVD synthesis for its larger domain sizes, universal and easy-to-use polymer-free transfer techniques must be developed as well.

Introduction

As a one-atom-thick material, graphene has become one of the main focuses of materials research owing to its extraordinary physical, chemical and electronic properties.[1] Among different synthetic techniques for graphene,[2–6] the chemical vapor deposition (CVD) approach of hydrocarbons on Cu substrates[6–8] has demonstrated the best graphene yield with the highest uniformity, largest film size and comparable quality with that derived by mechanical microcleavage.[1,9] However, a disadvantage of the CVD method is that after growth, a transfer process of graphene from Cu to the substrates of interests is required before the practical applications such as field-effect transistors (FETs).[10] A most popular transfer method is the 'wet transfer' that uses a polymer film covering graphene—such as poly(-methyl methacrylate) (PMMA)—as a protection layer and removes the underneath Cu substrate within an etchant solution, followed by picking up the isolated polymer/graphene layer onto other surfaces and dissolving the polymer with a proper solvent.[6] However, due to the introduction of the polymer layer onto the graphene surface, the quality of as-grown graphene is significantly reduced by various additional effects, for instance, the polymer residues always lead to a reduction of graphene's electronic performance, the strain and stress in graphene during transfer generate new wrinkles and other defects, and so on.[11–13] However, so far most of the previous reports have focused on the quality of transferred graphene after the polymer is removed,[14–18] and few of them have studied the influence of other factors such as the etchant solution[19] or the polymer layer. A systematic investigation on how each step during the wet transfer affects the quality of as-grown graphene is of high importance for the further improvement of the transfer techniques and the resultant graphene quality. Therefore, it is desirable to characterize the quality evolution of graphene step-by-step during the wet transfer.

On the other hand, Raman spectroscopy is a powerful and nondestructive tool for the rapid analysis of graphene.[20–22] The Raman spectrum of a graphene sample exhibits three featured peaks known as D, G, and 2D peaks which are very sensitive to external stimuli such as defects,[23–26] doping,[27,28] strain,[29–31] magnetic fields,[32,33] temperature,[34] *etc.* Therefore, collecting Raman signals and contour maps from graphene can behave as a fast and efficient approach to monitor its quality during and after the wet transfer process.

In this study, we use scanning Raman spectroscopy to monitor as-grown graphene during each step of wet transfer including floating on etchant solution, loaded onto a target substrate, and with additional annealing. Results show that the etchant solution results in strong compressive strain and p-type doping to floating graphene, but both are significantly reduced after the sample is loaded and rinsed especially for the doping. An annealing treatment increases the compressive strain in

[a]*Center for X-Mechanics and Institute of Applied Mechanics, Zhejiang University, Hangzhou 310012, P. R. China. E-mail: peizhao@zju.edu.cn; htw@zju.edu.cn*

[b]*Institute of Microelectronics, Chinese Academy of Sciences, Beijing 100029, China*

† Electronic supplementary information (ESI) available. See DOI: 10.1039/c9ra09268d

graphene but hardly its doping level. Moreover, when a PMMA layer is used to assist the transfer, it does not only increase the p-type doping of floating graphene but also lowers the crystalline quality of annealed graphene. Therefore, to obtain graphene with better quality, transfer of graphene without polymer protection needs to be considered.

Results and discussion

The schematic of direct (polymer-free, red arrows) and PMMA-assisted (blue arrows) transfer routes for graphene onto SiO_2/Si substrates is shown in Fig. 1a. The direct transfer includes three key steps of floating graphene (f-Gr), graphene loaded on a SiO_2/Si substrate (Gr) and annealed graphene on a SiO_2/Si substrate (Gr-A). For PMMA-assisted transfer, it starts with the spin-coating of a PMMA layer onto graphene, followed by floating PMMA/graphene (f-P/Gr), graphene loaded on a SiO_2/Si substrate after PMMA removal (P/Gr, the most widely studied case by researchers), and annealed graphene on a SiO_2/Si transferred in the previous step (P/Gr-A). Our focus in this work is the samples during/after the six steps of f-Gr, Gr, Gr-A, f-P/Gr, P/Gr and P/Gr-A. It needs to be mentioned that as-grown graphene on Cu is not studied here mainly due to that the strong fluorescence from Cu makes it difficult to obtain the accurate spectrum from graphene, as shown in Fig. S1, ESI.† However, considering that all the samples used in this work are synthesized using the same CVD recipe with the same initial quality, as well as that the first crucial step in wet transfer of graphene is to remove the Cu substrate by an etchant solution, it is reasonable that we start our analysis by comparing the floating graphene samples. The up and down panels in Fig. 1b show the experimental setups of f-Gr and f-P/Gr, respectively, including photographs of the floating samples on $FeCl_3$ solution from the top and side views, and their optical microscopy (OM) images. The graphene size adopted in our experiments is approximately 2 cm by 2 cm, similar to that in most lab tests. Compared with f-Gr that without a PMMA layer, f-P/Gr exhibits more apparent edges in the top view photograph and an optical birefringence from the PMMA layer. Typical Raman spectra measured from f-Gr, Gr, Gr-A, f-P/Gr, P/Gr and P/Gr-A are presented in Fig. 1c. It needs to be mentioned that for f-Gr, *n*-heptane is adopted to assist stabilizing the graphene film. The Raman spectrum of *n*-heptane derived directly from its liquid is shown in Fig. S2, ESI,† whose peaks are mainly distributed within 1300 to 1450 cm^{-1} and not overlap the peaks for graphene, and more importantly, during the experiments a much lower amount of *n*-heptane is used and its peaks are all negligible when compared with those from graphene.

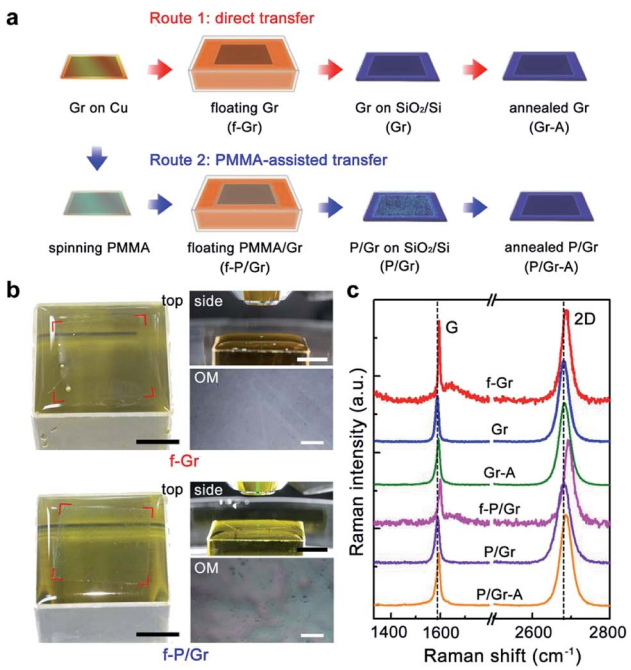

Fig. 1 (a) Schematic of direct and PMMA-assisted routes for wet transfer. The samples involved in this work are defined here as well. (b) Photographs (top and side views) and OM images of floating samples. Scale bars for digital images and OM images are 1 cm and 10 μm, respectively. (c) Typical Raman spectra measured from graphene samples defined in (a). The dash lines across the G and 2D center positions of a P/Gr sample indicate the reference of peaks shifts.

For all these spectra, only G (~1590 cm^{-1}) and 2D (~2680 cm^{-1}) peaks are observed without apparent D (~1350 cm^{-1}) peaks, indicating the high quality of these samples through our experiments.[22] Notably, for f-P/Gr even with a PMMA layer (~200–300 nm thick) covering on top, clear Raman signals can still be collected within the range of interest (1300–2800 cm^{-1}). Moreover, in both f-Gr and f-P/Gr a relatively weak and broad fluorescence peak located at ~1650 cm^{-1} is observed. Therefore, all the obtained G and 2D peaks are carefully fitted by Lorentzians after the spectrum decomposition.

More importantly, the centers of the G and 2D peaks in Fig. 1c are not at the same position as we draw reference lines across the G and 2D peak centers of the P/Gr spectrum especially for the two floating samples of f-Gr and f-P/Gr. These peak shifts are usually originated from the modifications of graphene lattices and/or the electronic structure. For instance, a compressive/tensile strain results in a blueshift/redshift for both the G and 2D peaks,[30,31] a p-type doping results in a blueshift for both peaks, and an n-type doping leads to a redshift for the 2D peak but blueshift for the G peak.[28] Such effects to graphene in each transfer step will be discussed in more details below.

Fig. 2 presents the Raman maps for f-Gr, Gr, Gr-A, f-P/Gr, P/Gr and P/Gr-A, including their G peak center positions, G peak full-width-at-half-maximum (FWHM), 2D peak center positions and 2D peak FWHM. These maps are listed in two panels, with the direct transfer on the left and PMMA-assisted transfer on the right. In each panel, the process flow of transfer steps is listed from left to right, so that the evolution of graphene's Raman peaks during the transfer is shown in this way as well. During the direct transfer, when graphene is picked up from solution onto a substrate, both its G and 2D peaks redshift by ~7 cm^{-1}, whereas their widths maintain almost the same. With additional annealing, its G peak blueshifts by ~5 cm^{-1} and 2D peak blueshifts by ~4 cm^{-1}, and both peak widths are broadened by ~2 cm^{-1}. On the other hand, during PMMA-assisted

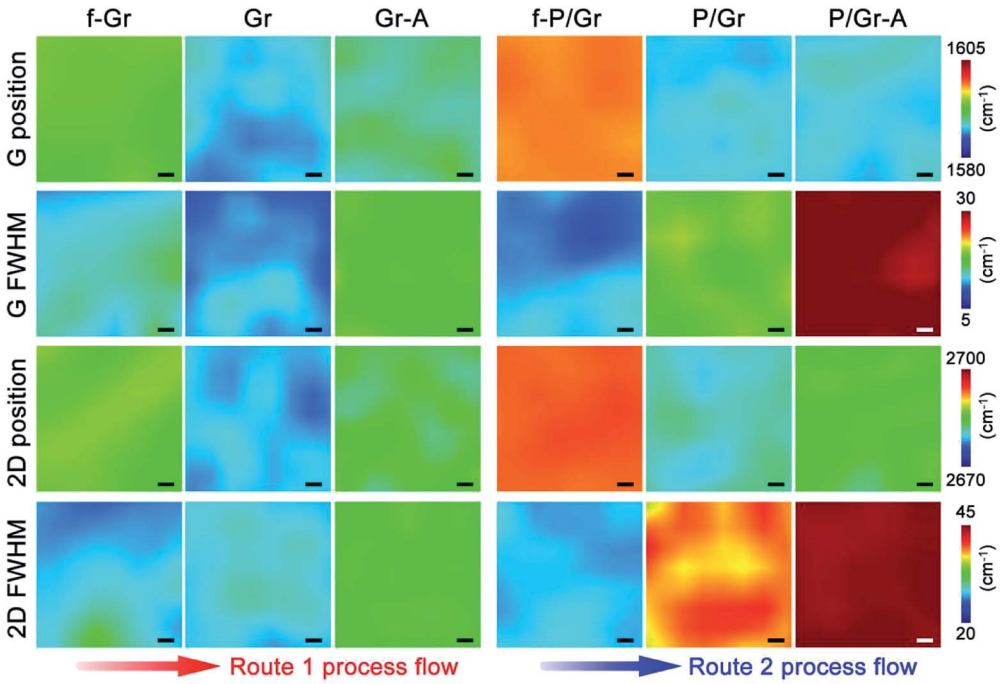

Fig. 2 Raman maps for f-Gr, Gr, Gr-A, f-P/Gr, P/Gr and P/Gr-A, including their G peak center positions, G peak FWHM, 2D peak center positions and 2D peak FWHM. The results from a direct transfer is shown in the left panel and those from PMMA-assisted transfer in the right panel. All scale bars: 10 μm.

transfer, compared with floating graphene without PMMA, both the G and 2D peaks of floating graphene with PMMA significantly blueshift by ~7 cm^{-1}, but their peak widths are slightly narrower by ~2 cm^{-1}. After the sample is picked up and the removal of PMMA, its G peak redshifts by ~10 cm^{-1} and 2D peak by ~12 cm^{-1}, to the positions almost the same as those of graphene by the direct transfer. However, the widths of these peaks are broadened by 5 cm^{-1} and 13 cm^{-1} for the G and 2D peaks, respectively, much broader than those from graphene by direct transfer. A more considerable change occurs when this sample is further annealed. Although the G peak maintains its position and the 2D peak slightly blueshifts by 3 cm^{-1}, the widths of both peaks are significantly increased by 10 cm^{-1} and 12 cm^{-1}, respectively.

These results imply that compared with graphene by direct transfer, when PMMA is used graphene experiences a higher level of external strain from the environment and/or doping from the contact agents.[28,30,31] In Fig. 3 we collect the data of graphene from above maps and summarize them using scatter plots of the peak width against the peak center position for the G and 2D peaks. Here we discuss these peak widths first. Apparently, graphene samples floating on the etchant solution (f-Gr and f-P/Gr) exhibit the smallest peak widths. Considering the width of a generated peak is usually inversely proportional to phonon lifetime and proportional to phonon scattering rate,[35,36] the narrow peaks from f-Gr and f-P/Gr are indicative of their high crystalline structure with fewer scattering sites for phonons. These scattering sites are usually defects and impurities in graphene that are different from the sp^2-carbon honeycomb-like crystalline structures.[37,38] After they are picked up onto substrates, with or without PMMA their G and 2D peak widths are both broadened. We attribute such broadening to the increased phonon scattering by the existence of a supporting substrate. Moreover, the peak widths of graphene transferred with PMMA are broadened by a larger extent, suggesting that the removal of PMMA lowers the structural quality of graphene by leaving residues or creating defects in graphene as new scattering sites,[14] but they are too few to be detected by the Raman D peaks. After annealing, for direct transferred graphene both its G and 2D peak widths maintain the same, indicating that the sample quality is not affected by such

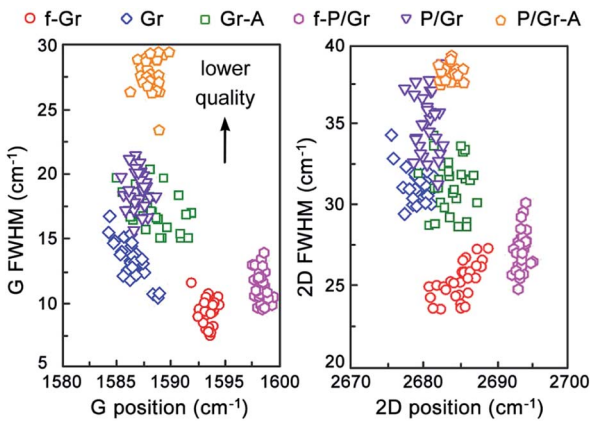

Fig. 3 Scatter plots of peak width against peak center position for the G and 2D peaks of graphene at different steps during direct and PMMA-assisted transfer.

treatment. However, for graphene transferred with PMMA, its both peaks are broadened after the annealing, especially for the G peak. As demonstrated in previous reports, the main propose of annealing is to remove polymer residues attached on the graphene surface.[14,39] Cheng *et al.* demonstrated that the removal of PMMA can result in sp^3-type point defects formed by polymer residues with carbon atoms in graphene.[40] Therefore, it is safe to conclude that such residue removal by annealing actually results in more scattering of phonons in graphene, probably due to the loss of carbon atoms together with polymer residues.

Now we turn to the discussion of peak shifting during the transfer of graphene. As we mentioned previously, both strain and doping can result in shift of Raman peaks.[27–31] In Fig. 4 we plot a correlation map of the G and 2D peak positions for graphene at each step of direct and PMMA-assisted transfer. Two solid lines indicative of zero doping (left) and zero strain (right) are shown across the map as well, with the arrow directions pointing to the increase of 'pure' compressive strain and p-type doping, respectively. In other words, graphene with Raman peak positions located on these lines can be considered as being affected only by strain or doping. These two lines are derived based on the data from ref. 18 and 29, respectively, and the cross point of these lines indicates the neutral state of graphene. Previous studies have demonstrated that CVD graphene are subject to nonuniform compressive strains resulted from the mismatch of graphene and Cu lattices.[41,42] For both floating graphene, they are under a combined state of compressive strain and p-type doping, and f-P/Gr exhibits much higher strain and doping levels than f-Gr, resulted from the strong constraint effect and charge transfer to graphene by PMMA, respectively.[18] After picked up onto a SiO_2/Si substrate, through each route the doping in graphene can be largely reduced to almost zero, but the compressive strain is maintained although it is significantly reduced. The compression state of graphene by PMMA-assisted transfer is consistent with the previous reports. With further annealing, the compressive strain in both Gr and P/Gr increases, but no apparent doping from the SiO_2/Si substrates is observed, much smaller than the previous results by Kong *et al.*, in which a doping effect from the underlying SiO_2/Si can be transferred to graphene.[18,28]

Finally, we discuss more on the annealing treatment to transferred graphene. Annealing is usually considered as an efficient way to improve the electrical performance of transferred graphene by further removing the polymer residues and enhance the contact between graphene and the substrate.[28] However, our above results clearly demonstrate that annealing will result in the lowering of graphene's crystalline quality, probably due to the loss of carbon atoms together with polymer residues. To test the electrical performance of annealed graphene, we measured the sheet resistance of transferred graphene before and after annealing, for samples by direct and PMMA-assisted transfer. The results are presented in Fig. 5. Without PMMA, the sheet resistance of transferred graphene is ~590–860 Ω $\square^{-1}$, which is reduced to ~370–650 Ω $\square^{-1}$ after annealing. On the other hand, with PMMA involved, the sheet resistance of transferred graphene is ~900–1050 Ω $\square^{-1}$, and is reduced to ~720–810 Ω $\square^{-1}$ by annealing. Apparently, although with the probability of lowering the crystalline quality of graphene, annealing still behaves as a promising way to improve the graphene electrical conductivity. However, the negative effects in both the crystallinity and the electrical performance from the PMMA protection layer must be eliminated, and universal and easy-to-use polymer-free transfer techniques must be developed in the future of graphene research.

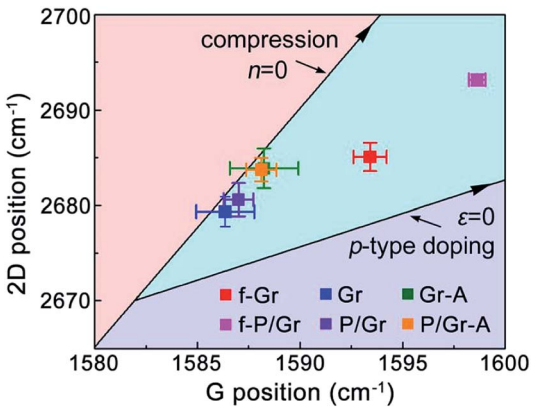

Fig. 4 A correlation map of the G and 2D peak positions of graphene at different steps in direct and PMMA-assisted transfer.

Experimental

Graphene synthesis

Polycrystalline graphene was synthesized on commercially available Cu (Suzhou Fukuda Metal Co. Ltd) foils using a low-pressure CVD process.[6] In details, a Cu foil was loaded into the CVD quartz chamber and heated to 1060 °C within a H_2 atmosphere for 70 min, to remove the metal surface impurities and increase the metal grain size. A self-limiting growth of monolayer graphene was then conducted using 10 sccm H_2 and 1 sccm CH_4 for 30 min.

Graphene transfer

For direct (polymer-free) transfer of graphene, a 1 M $FeCl_3$ aqueous solution was slightly overloaded in a container to form a convex liquid surface, on which the CVD-grown graphene/Cu foil was carefully floated. The graphene surface was then covered by several drops of *n*-heptane as a liquid protection layer. After the Cu foil was etched, isolated graphene was directly printed and picked up using a SiO_2 (300 nm)/Si substrate and rinsed by deionized water.

For PMMA-assisted transfer, a thin layer of PMMA (4 wt% in anisole, AR-P 679.04, Allresist GmbH, Germany) was spin-coated onto as-grown graphene on a Cu foil at a speed of 3000 rpm and baked at 105 °C. The same amount of $FeCl_3$ as the direct transfer was used, and after the total removal of the Cu foil, the isolated graphene/PMMA film was rinsed and loaded

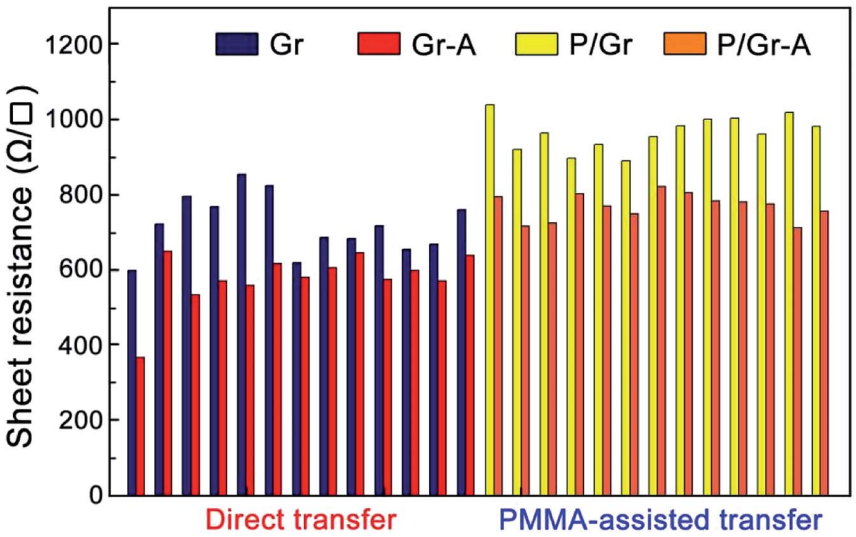

Fig. 5 Sheet resistance of graphene samples before and after the annealing treatments transferred by polymer-free or PMMA-assisted methods.

onto a SiO_2/Si substrate, and the PMMA layer was then removed by dichloromethane at 45 °C.

The annealing treatment of transferred graphene was conducted by placing the samples in a clean CVD quartz tube at 360 °C with 100 sccm H_2 for 6 hours.

Raman measurements and other characterizations

The Raman spectra and maps were collected using confocal micro-Raman spectroscopy (LabRAM HR Evolution, Horiba Co. Ltd.) with a laser excitation wavelength of 532 nm and a power of 12.5 mW. A long-focal length 50× objective lens with NA = 0.95 and standard grating (1800 grad per mm) were used, and the laser spot size was estimated to be 1.4 μm. The Raman spectra had a resolution of <0.5 cm^{-1} and the spatial resolution in all the Raman maps was as 5 μm. All the measured spectral data were analyzed using the LabSpe6 software.

For graphene sheet resistance measurements, standard four-point probe technique at room temperature was used. The interval distances between the linearly arranged probes were 1 mm, and each sample was measured for more than ten times.

Conclusions

In summary, we have used scanning Raman spectroscopy as an efficient tool to resolve the quality evolution of as-grown graphene during wet transfer, by monitoring the shift of the center position and width of Raman G and 2D peaks collected from graphene at each step during transfer: floating on etchant solution, loaded onto a target substrate, and with additional annealing. Results show that the etchant solution results in strong compressive strain and p-type doping to floating graphene, but both are significantly reduced after the sample is picked up and rinsed especially for the doping. Annealing increases the compression level in graphene but hardly increases its doping level. Moreover, when a PMMA layer is used to assist the transfer, it does not only increase the p-type doping of floating graphene but also lowers the crystalline quality of annealed graphene as indicated by the largely broadened Raman peak width. Therefore, to obtain graphene with better quality, besides the attempts of improving CVD synthesis for its larger domain sizes, universal and easy-to-use polymer-free transfer techniques must also be developed.

Conflicts of interest

There are no conflicts to declare.

Acknowledgements

This work was financially supported by the National Key Scientific Instruments and Equipment Development Project of China (61427901) and the National Natural Science Foundation of China (11872330, 11574268).

Notes and references

1 K. S. Novoselov, V. I. Falko, L. Colombo, P. R. Gellert, M. G. Schwab and K. Kim, *Nature*, 2012, **490**, 192–200.
2 K. S. Novoselov, D. Jiang, F. Schedin, T. J. Booth, V. V. Khotkevich, S. V. Morozov and A. K. Geim, *Proc. Natl. Acad. Sci. U.S.A.*, 2005, **102**, 10451–10453.
3 S. Stankovich, D. A. Dikin, R. D. Piner, K. A. Kohlhaas, A. Kleinhammes, Y. Jia, Y. Wu, S. T. Nguyen and R. S. Ruoff, *Carbon*, 2007, **45**, 1558–1565.
4 C. Berger, Z. Song, X. Li, X. Wu, N. Brown, C. Naud, D. Mayou, T. Li, J. Hass, A. N. Marchenkov, E. H. Conrad, P. N. First and W. A. de Heer, *Science*, 2006, **312**, 1191–1196.
5 K. S. Kim, Y. Zhao, H. Jang, S. Y. Lee, J. M. Kim, K. S. Kim, J. H. Ahn, P. Kim, J. Y. Choi and B. H. Hong, *Nature*, 2009, **457**, 706–710.

6 X. Li, W. Cai, J. An, S. Kim, J. Nah, D. Yang, R. Piner, A. Velamakanni, I. Jung, E. Tutuc, S. K. Banerjee, L. Colombo and R. S. Ruoff, *Science*, 2009, **324**, 1312–1314.
7 Y. Hao, M. S. Bharathi, L. Wang, Y. Liu, H. Chen, S. Nie, X. Wang, H. Chou, C. Tan, B. Fallahazad, H. Ramanarayan, C. W. Magnuson, E. Tutuc, B. I. Yakobson, K. F. McCarty, Y.-W. Zhang, P. Kim, J. Hone, L. Colombo and R. S. Ruoff, *Science*, 2013, **342**, 720–723.
8 X. Xu, Z. Zhang, J. Dong, D. Yi, J. Niu, M. Wu, L. Lin, R. Yin, M. Li, J. Zhou, S. Wang, J. Sun, X. Duan, P. Gao, Y. Jiang, X. Wu, H. Peng, R. S. Ruoff, Z. Liu, D. Yu, E. Wang, F. Ding and K. Liu, *Sci. Bull.*, 2017, **62**, 1074–1080.
9 N. Petrone, C. R. Dean, I. Meric, A. M. van der Zande, P. Y. Huang, L. Wang, D. Muller, K. L. Shepard and J. Hone, *Nano Lett.*, 2012, **12**, 2751–2756.
10 Y. Chen, X.-L. Gong and J.-G. Gai, *Adv. Sci.*, 2016, **3**, 1500343.
11 E. Koo and S.-Y. Ju, *Carbon*, 2015, **86**, 318–324.
12 A. Pirkle, J. Chan, A. Venugopal, D. Hinojos, C. W. Magnuson, S. McDonnell, L. Colombo, E. M. Vogel, R. S. Ruoff and R. M. Wallace, *Appl. Phys. Lett.*, 2011, **99**, 122108.
13 N. Liu, Z. Pan, L. Fu, C. Zhang, B. Dai and Z. Liu, *Nano Res.*, 2011, **4**, 996–1004.
14 X. Liang, B. A. Sperling, I. Calizo, G. Cheng, C. A. Hacker, Q. Zhang, Y. Obeng, K. Yan, H. Peng, Q. Li, X. Zhu, H. Yuan, A. R. Hight Walker, Z. Liu, L.-M. Peng and C. A. Richter, *ACS Nano*, 2011, **5**, 9144–9153.
15 J. Song, F.-Y. Kam, R.-Q. Png, W.-L. Seah, J.-M. Zhuo, G.-K. Lim, P. K. H. Ho and L.-L. Chua, *Nat. Nanotechnol.*, 2013, **8**, 356–362.
16 S. Kim, S. Shin, T. Kim, H. Du, M. Song, C. Lee, K. Kim, S. Cho, D. H. Seo and S. Seo, *Carbon*, 2016, **98**, 352–357.
17 H. Sun, D. Chen, Y. Wu, Q. Yuan, L. Guo, D. Dai, Y. Xu, P. Zhao, N. Jiang and C.-T. Lin, *J. Mater. Chem. C*, 2017, **5**, 1880–1884.
18 W. S. Leong, H. Wang, J. Yeo, F. J. Martin-Martinez, A. Zubair, P.-C. Shen, Y. Mao, T. Palacios, M. J. Buehler, J.-Y. Hong and J. Kong, *Nat. Commun.*, 2019, **10**, 867.
19 C. Bautista-Flores, R. Y. Sato-Berrú and D. Mendoza, *Mater. Res. Express*, 2018, **6**, 015601.
20 J.-B. Wu, M.-L. Lin, X. Cong, H.-N. Liu and P.-H. Tan, *Chem. Soc. Rev.*, 2018, **47**, 1822–1873.
21 B. Tang, H. Guoxin and H. Gao, *Appl. Spectrosc. Rev.*, 2010, **45**, 369–407.
22 L. M. Malard, M. A. Pimenta, G. Dresselhaus and M. S. Dresselhaus, *Phys. Rep.*, 2009, **473**, 51–87.
23 A. C. Ferrari, *Solid State Commun.*, 2007, **143**, 47–57.
24 L. G. Cancado, A. Jorio, E. H. Martins Ferreira, F. Stavale, C. A. Achete, R. B. Capaz, M. V. O. Moutinho, A. Lombardo, T. S. Kulmala and A. C. Ferrari, *Nano Lett.*, 2011, **11**, 3190–3196.
25 M. M. Lucchese, F. Stavale, E. H. M. Ferreira, C. Vilani, M. V. O. Moutinho, R. B. Capaz, C. A. Achete and A. Jorio, *Carbon*, 2010, **48**, 1592–1597.
26 P. Venezuela, M. Lazzeri and F. Mauri, *Phys. Rev. B: Condens. Matter Mater. Phys.*, 2011, **84**, 035433.
27 A. Das, S. Pisana, B. Chakraborty, S. Piscanec, S. K. Saha, U. V. Waghmare, K. S. Novoselov, H. R. Krishnamurthy, A. K. Geim, A. C. Ferrari and A. K. Sood, *Nat. Nanotechnol.*, 2008, **3**, 210–215.
28 M. Kalbac, H. Farhat, J. Kong, P. Janda, L. Kavan and M. S. Dresselhaus, *Nano Lett.*, 2011, **11**, 1957–1963.
29 Y. Wang, Y. Wang, C. Xu, X. Zhang, L. Mei, M. Wang, Y. Xia, P. Zhao and H. Wang, *Carbon*, 2018, **134**, 37–42.
30 M. Huang, H. Yan, C. Chen, D. Song, T. F. Heinz and J. Hone, *Proc. Natl. Acad. Sci. U.S.A.*, 2009, **106**, 7304–7308.
31 T. M. G. Mohiuddin, A. Lombardo, R. R. Nair, A. Bonetti, G. Savini, R. Jalil, N. Bonini, D. M. Basko, C. Galiotis, N. Marzari, K. S. Novoselov, A. K. Geim and A. C. Ferrari, *Phys. Rev. B: Condens. Matter Mater. Phys.*, 2009, **79**, 205433.
32 C. Faugeras, M. Amado, P. Kossacki, M. Orlita, M. Sprinkle, C. Berger, W. A. de Heer and M. Potemski, *Phys. Rev. Lett.*, 2009, **103**, 186803.
33 T. Ando, *J. Phys. Soc. Jpn.*, 2007, **76**, 024712.
34 T. G. A. Verhagen, K. Drogowska, M. Kalbac and J. Vejpravova, *Phys. Rev. B: Condens. Matter Mater. Phys.*, 2015, **92**, 125437.
35 A. Jorio, R. Saito, G. Dresselhaus and M. S. Dresselhaus, *Raman spectroscopy in graphene related systems*, Wiley-VCH Verlag GmbH & Co. KGaA, 2011.
36 P. Zhao, E. Einarsson, R. Xiang, Y. Murakami, S. Chiashi, J. Shiomi and S. Maruyama, *Appl. Phys. Lett.*, 2011, **99**, 093104.
37 A. C. Ferrari, *Solid State Commun.*, 2007, **143**, 47.
38 C. Casiraghi, S. Pisana, K. S. Novoselov, A. K. Geim and A. C. Ferrari, *Appl. Phys. Lett.*, 2007, **91**, 233108.
39 Z. Cheng, Q. Zhou, C. Wang, Q. Li, C. Wang and Y. Fang, *Nano Lett.*, 2011, **11**, 767–771.
40 Y. Lin, C. Lu, C. Yeh, C. Jin, K. Suenage and P. Chiu, *Nano Lett.*, 2012, **12**, 414–419.
41 R. He, L. Zhao, N. Petrone, K. S. Kim, M. Roth, J. Hone, P. Kim, A. Pasupathy and A. Pinczuk, *Nano Lett.*, 2012, **12**, 2408–2413.
42 V. Yu, E. Whiteway, J. Maassen and M. Hilke, *Phys. Rev. B: Condens. Matter Mater. Phys.*, 2011, **84**, 205407.